applied sciences

MDPI

Article

Effects of La-Co Co-Substitution on the Structural and Magnetic Properties of SrM Hexaferrites Prepared by Solid-State Reaction

Kanghyuk Lee [1], Young-Min Kang [2] and Sang-Im Yoo [1,*]

[1] Department of Materials Science and Engineering, Research Institute of Advanced Materials (RIAM), Seoul National University, Seoul 08826, Republic of Korea
[2] Department of Materials Science & Engineering, Korea National University of Transportation, Chungju 27469, Republic of Korea
* Correspondence: siyoo@snu.ac.kr

Abstract: The effects of La-Co co-substitution on the structural and magnetic properties of strontium M-type hexaferrites (SrM) were carefully investigated for the $Sr_{1-x}La_xFe_{12-x}Co_xO_{19}$ ($0.0 \leq x \leq 0.3$) polycrystalline samples prepared by solid-state reaction in air. Without the use of sintering additives, La-Co co-substituted SrM single phases could be obtained from polycrystalline bulk samples by employing proper processing conditions. The lattice parameter a initially increases with increasing x from 0.0 to 0.1 but gradually decreases with increasing x to 0.20, and then remains almost unaltered up to $x = 0.3$; the lattice parameter c monotonously decreases with increasing x from 0.0 to 0.25, but it turns to an increase when $x = 0.3$. The reduction in c/a ratios and V_{cell} values with increasing x up to $x = 0.25$ are obviously attributable to the decreasing size effect resulting from La^{3+} substitution at the Sr^{2+} site, which surpasses the increasing size effect due to Co^{2+} and Fe^{2+} occupancy at the Fe^{3+} site. Meanwhile, with increasing x from 0.0 to 0.3, while the saturation magnetization (M_S) continuously decreases from 75.90 to 72.07 emu/g, the magnetic anisotropy field (H_a) increases from 20.1 to 24.7 kOe, leading to an increase in the intrinsic coercivity (H_{ci}) from 2.68 to 3.99 kOe. The gradual increase in H_a with x, probably caused by a gradual decrease in the crystallographic symmetry, is inversely proportional to the variation in the c/a ratios up to $x = 0.25$ as usual except when $x = 0.3$, of which deviation needs further study.

Keywords: SrM-type hexaferrites; La-Co substitution; saturation magnetization; magnetic anisotropy field; intrinsic coercivity

check for updates

Citation: Lee, K.; Kang, Y.-M.; Yoo, S.-I. Effects of La-Co Co-Substitution on the Structural and Magnetic Properties of SrM Hexaferrites Prepared by Solid-State Reaction. *Appl. Sci.* **2024**, *14*, 848. https://doi.org/10.3390/app14020848

Academic Editor: Philippe Lambin

Received: 15 December 2023
Revised: 15 January 2024
Accepted: 15 January 2024
Published: 19 January 2024

Copyright: © 2024 by the authors. Licensee MDPI, Basel, Switzerland. This article is an open access article distributed under the terms and conditions of the Creative Commons Attribution (CC BY) license (https://creativecommons.org/licenses/by/4.0/).

1. Introduction

Hexagonal ferrites, such as $BaFe_{12}O_{19}$ (BaM) and $SrFe_{12}O_{19}$ (SrM), are commercially important as ceramic permanent magnets for industrial applications due to their cost-effectiveness, strong uniaxial magnetic anisotropy along the *c*-axis, and excellent chemical stability [1]. The BaM hexaferrite and SrM hexaferrite, which have the same crystal structure as the magnetoplumbite mineral, were discovered in the early 1950s by Philips [2,3]. It was found that SrM hexaferrite has better magnetic properties than BaM at room temperature [4,5]. These M-type hexaferrites are typically prepared by solid-state reaction [1] because this process is cost-effective and suitable for mass production [6].

The performance of a permanent magnet can be evaluated by its remanent flux density (B_r), coercivity (H_c), and maximum energy product $(BH)_{max}$. These properties are extrinsic and depend on the microstructure, including sintered density, average grain size, and degree of grain alignment. However, these parameters are closely related to intrinsic properties such as magnetization saturation (M_S) and uniaxial crystal anisotropy constant (K_u). These properties depend on the composition of the substituted cation and their occupancy on each site within the unit cell [6,7]. Although high values of B_r and $(BH)_{max}$ can be obtained from a highly dense, small-grained sample with a microstructure that is

highly textured along the easy axis, it is necessary to use a composition with higher M_S and K_u values. This is because the B_r value is limited to the saturation magnetic induction (B_s) on the B-H loop, which corresponds to the M_S value on the M-H curve. Additionally, the H_c value depends not only on the grain size but also on K_u [1,8,9]. Sometimes, the magnetic anisotropy field (H_a) is a more convenient representation of the strength of magnetic anisotropy along the easy axis than K_u because H_a is proportional to K_u, as shown by the relationship $H_a = 2K_u/M_S$ for a spherical single domain particle [10].

Numerous studies have been conducted to improve the intrinsic magnetic properties of SrM hexaferrites through cation substitutions. Co [11], Ti [12], Al [13], and Zn [14] have been substituted for the Fe sites, while La [15], Nd [16], and Sm [16] have been substituted for the Sr sites. Among these substituents, La-Co co-substitution has been found to be very effective in improving H_a without significantly decreasing M_s. However, previous reports on the effect of La-Co co-substitution for SrM on the structural parameters, including the lattice parameters and unit cell volume, as well as the intrinsic magnetic properties of M_s and H_a, are not in good agreement with each other [17–23]. The M_s value increased gradually with increasing La-Co co-substitution (x) up to $x = 0.3$ [18], or it increased up to $x = 0.2$ and then decreased with further increasing x [19], or it decreased continuously [20]. The variation in H_a with x showed a common tendency; H_a increased gradually with increasing x, although there was a significant difference in the H_{ci} values [17–23]. This difference in the intrinsic magnetic properties of La-Co co-substituted SrM is likely due to the sintering additives such as SiO_2 [18,21,24], $CaCO_3$ [18,21], and Bi_2O_3 [19]. According to reports, Ca can substitute for Sr sites [25], while Si [26] and Bi [27] can substitute for Fe sites in M-type hexaferrites. This suggests that the kind and amount of sintering additives can affect M_S and H_a. To identify the intrinsic magnetic properties of La-Co co-substituted SrM hexaferrites without using sintering additives, it is necessary to prepare samples consisting of a single phase of M-type without any second phase.

Previous reports [17,20,23,28] have investigated La-Co co-substituted SrM samples without using sintering additives. Polycrystalline samples were prepared through solid-state reaction [17], powder samples were prepared through the sol-gel process and subsequent heat treatment [20,23], and single crystals were grown through the flux growth method [28]. However, their results are not in good agreement. T. Kikuchi et al. [20] reported that it is possible to synthesize M-type single-phase powder with the same amount of La and Co (i.e., the molar ratio of Co/La = 1.0) up to $x = 0.4$ by using the sol–gel process and subsequent heat treatment at 900 °C for 24 h in air. On the other hand, T. Wake et al. [17] reported that the Co/La molar ratios of samples sintered at 1300–1350 °C for 24 h in air decreased to less than 1. For x values greater than 0.1, the deviation increased. This trend of La-Co co-substitution with a relatively larger amount of La relative to Co has also been observed for flux-grown single crystals in air [28]. To achieve a single-phase M-type structure in La-Co-substituted SrM through solid-state reactions without the use of additives is a difficult challenge. However, it is essential to determine the crystal structure and magnetic properties of La-Co-substituted SrM without sintering additives for research purposes. This is important for understanding lattice constants, M_S, and H_a, as reported in previous research.

To clarify this discrepancy, in this study we attempted to prepare La-Co co-substituted SrM polycrystalline samples of the M-type single phase by solid-state reaction without using sintering additives. We report and discuss the structural and magnetic properties of samples fabricated up to $x = 0.3$ in $Sr_{1-x}La_xFe_{12-x}Co_xO_{19}$.

2. Materials and Methods

The La-Co co-substituted SrM hexaferrites were prepared by solid-state reaction in air. The precursors used were $SrCO_3$, Fe_2O_3, La_2O_3, and Co_3O_4 powders (all 99.9% purity) with a nominal composition of $Sr_{1-x}La_xFe_{12-x}Co_xO_{19}$, where $0.0 \leq x \leq 0.4$. The $SrCO_3$ and Fe_2O_3 powders were first mixed and ball-milled with zirconia balls in ethanol for 24 h. The resulting powder mixture was then dried in an oven at 70 °C. The powder mixture

was dried and calcined at 1280 °C for 2 h in air with cation ratios of Sr:Fe = $(1-x)$:$(12-x)$. Subsequently, La_2O_3 and Co_3O_4 powders were added to the calcined powder, ball-milled for 24 h in an ethanol solution, and dried again. The dried powders were then pelletized using a uniaxial press (Jeil Hydraulics, Seoul, Republic of Korea) and sintered at 1300 °C for 2 h in air.

The densities of the sintered samples were calculated using Archimedes' principle (KERN & SOHN GmbH, Balingen, Germany). Powder X-ray diffraction (XRD) was performed using a Bruker D8 Advance instrument and a Cu Kα radiation source (λ = 0.15406 nm) for phase analysis and lattice parameter calculation. The lattice parameters a and c were calculated using Rietveld refinement. Microstructures of the samples were analyzed using field emission scanning electron microscopy (FE-SEM) with a ZEISS MERLIN Compact instrument (Zeiss, Oberkochen, Germany). To observe grain boundaries, polished samples were thermally etched in a muffle furnace at 1130 °C for 0.5 h in air. Initial magnetization and magnetic hysteresis (M-H) curves were measured at room temperature using a VSM (VSM-7410, Lakeshore, Westerville, OH, USA) with an applied field sweep within ± 26 kOe. Cube-shaped specimens with dimensions of approximately 2.0 × 2.0 × 2.0 mm were used for these measurements. The M_S and H_a values were determined from the initial magnetization curves, while the H_{ci} values were obtained from the *M-H* loops.

3. Results and Discussion

3.1. Crystalline Structure and Microstructure Analysis

Much effort has been devoted to identifying processing conditions that are suitable for the synthesis of the M-type single phase from samples with the nominal composition $Sr_{1-x}La_xFe_{12-x}Co_xO_{19}$ (x = 0.3). To achieve this, we initially followed the conventional solid-state reaction in air. All precursors were mixed, ball-milled, and calcined at 1280 °C for 2 h. The as-calcined powders were then ball-milled and pelletized before being sintered at 1300 °C for 2 h. Figure 1a (bottom) shows that obtaining the M-type single phase [SrM, JCPDS card 00-033-1340] was difficult due to the presence of second phases such as Fe_2O_3 [JCPDS card 04-008-7623], $CoFe_2O_4$ [JCPDS card 00-022-1086], and $LaFeO_3$ [JCPDS card 04-011-7994]. To address this issue, we modified our calcination process as described in the Experimental procedures. After the modified calcination process, the samples were sintered at 1230 °C for 2 h in air. This temperature and duration were found to be appropriate for obtaining the M-type single phase when using sintering additives of SiO_2 and $CaCO_3$, based on our independent experiments. However, as shown in Figure 1a (middle), it was not possible to obtain the M-type single phase. Instead, minor peaks of Fe_2O_3, $LaFeO_3$, and $CoFe_2O_4$ were always detectable. Subsequently, it was discovered that a sintering temperature of 1300 °C was necessary to prepare the M-type single phase without any second phase, as depicted in Figure 1a (top). Figure 1b shows the powder XRD patterns of $Sr_{1-x}La_xFe_{12-x}Co_xO_{19}$ ($0.0 \leq x \leq 0.4$) samples sintered at 1300 °C for 2 h. It is evident that the M-type single phase is obtainable from all samples up to x = 0.3. The XRD pattern for the sample of x = 0.4 sintered at 1300 °C for 2 h is shown in Figure 1b. Fe_2O_3, $CoFe_2O_4$, and $LaFeO_3$ minor peaks are detectable. The inability to obtain the M-type single phase from the x = 0.4 sample may be due to a kinetic limit in our fabrication process rather than the solubility limit of La-Co. T. Kikuchi et al. [20] reported that the M-type single phase was obtainable from the x = 0.4 sample through a sol–gel process and subsequent firing at a relatively low temperature of 900 °C for 24 h in air [20].

The present results are significantly different from those previously reported by T. Waki et al. [17], who prepared the samples by a solid-state reaction. According to their analysis of the contents of La and Co in La-Co co-substituted SrM samples sintered at 1300–1350 °C for 24 h in air, the molar ratio of Co/La is close to 1.0 for x = 0.1, but it gradually decreases with further increasing x. Their powder XRD patterns for the samples synthesized in air (see Figure 1a in ref. [17]) were also examined. From the XRD pattern analysis of samples with x values of 0.1 and 0.2, it is evident that they consist solely of the M-type single phase. However, samples with x values of 0.3 and 0.5 contain second phases

in addition to the M-type single phase. The XRD pattern of the sample with an x value of 0.2 shows that it is composed only of the M-type single phase. This suggests that the molar ratio of Co/La in this sample is at least close to 1.0. However, the analysis result (see Figure 3 in ref. [17]) indicates that it is significantly lower than 1.0, which may be difficult to comprehend. For instance, in the case of x = 0.3, the XRD pattern clearly shows the presence of a spinel phase (see Figure 1a in ref. [17]). Our XRD patterns in Figure 1b show only the M-type single phase, and no second phase was observed in their microstructure by SEM-EDS analyses. This strongly supports that the same amount of La and Co with the initial compositions are incorporated in the M-type single phase.

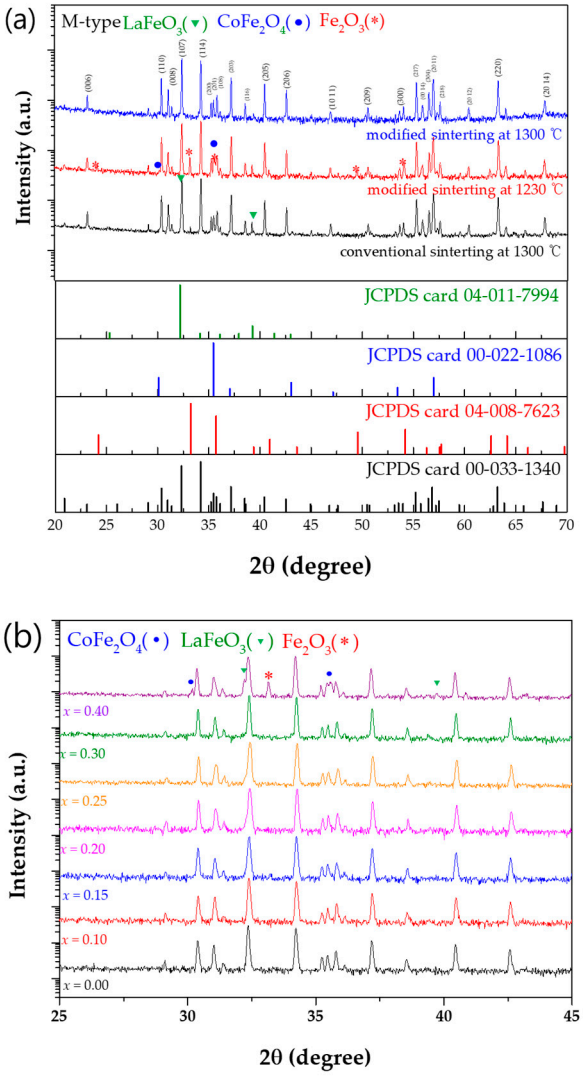


Figure 1. The powder XRD patterns of samples with x = 0.3 in $Sr_{1-x}La_xFe_{12-x}Co_xO_{19}$ as a representative of all samples are shown in (**a**), where bottom pattern is from the conventional process (calcination at 1280 °C for 2 h, sintering at 1300 °C for 2 h), middle pattern from our modified process (calcination at 1280 °C for 2 h, sintering at 1230 °C for 2 h), and top pattern from our modified process (calcination at 1280 °C for 2 h, sintering at 1300 °C for 2 h). Powder XRD patterns from our modified process (calcination at 1280 °C for 2 h, sintering at 1300 °C for 2 h) for the samples with x = 0, 0.1, 0.15, 0.2, 0.25, 0.3, and with x = 0.4 (**b**).

Meanwhile, our results are consistent with previous studies [20,23] on La-Co co-substituted SrM powder synthesized through the sol–gel process and subsequent heat treatment at 900 °C in air. T. Kikuchi et al. [20] were able to synthesize the M-type single phase up to x = 0.4 using this processing route, possibly due to a homogeneous mixture

of cation components that facilitated the formation of the M-type single phase. However, it should be noted that their samples consist of $Sr_{1.05-x}La_xFe_{12-x}Co_xO_{19}$ ($0.0 \leq x \leq 0.4$), which is equivalent to $Sr_{1-x}La_xFe_{11.43-x}Co_xO_{19}$ ($0.0 \leq x \leq 0.38$) in our notation. Although their samples only consist of the M-type single phase up to x = 0.4, their x value of 0.4 corresponds to 0.38 in our notation. Furthermore, it is difficult to directly compare their results with ours because they used 11.43 instead of 12 as the molar ratio of Fe/Sr. This suggests that about 5 mol% of Fe-deficient SrM was used for La-Co co-substitution.

To calculate the lattice parameters a and c, Rietveld refinement was performed with R_{wp} (weighted profile R-value) less than 9% and χ^2 (reduced Chi-squared value) less than 1.4 accuracy. The Rietveld analysis data are shown in Figure 2a,b for x = 0.0 and 0.3, respectively, as representatives of all samples. From the powder XRD patterns in Figure 1b, the lattice parameters a and c of the samples were calculated using the following equation [19],

$$d_{hkl} = \left\{ \frac{4\left(h^2 + hk + k^2\right)}{3a^2} + \frac{l^2}{c^2} \right\}^{-1/2} \quad (1)$$

where d_{hkl} is the inter-planer spacing and h, k, and l are the Miller indices. The cell volume (V_{cell}) values were calculated using $a^2c\sin120°$. The calculated lattice constants a and c, c/a ratios, and V_{cell} values for $Sr_{1-x}La_xFe_{12-x}Co_xO_{19}$ ($0.0 \leq x \leq 0.3$) samples are listed in Table 1. The a and c values of this table are plotted as a function of x in Figure 3a. The c/a ratios and V_{cell} values of this table are also plotted as a function of x in Figure 3b.

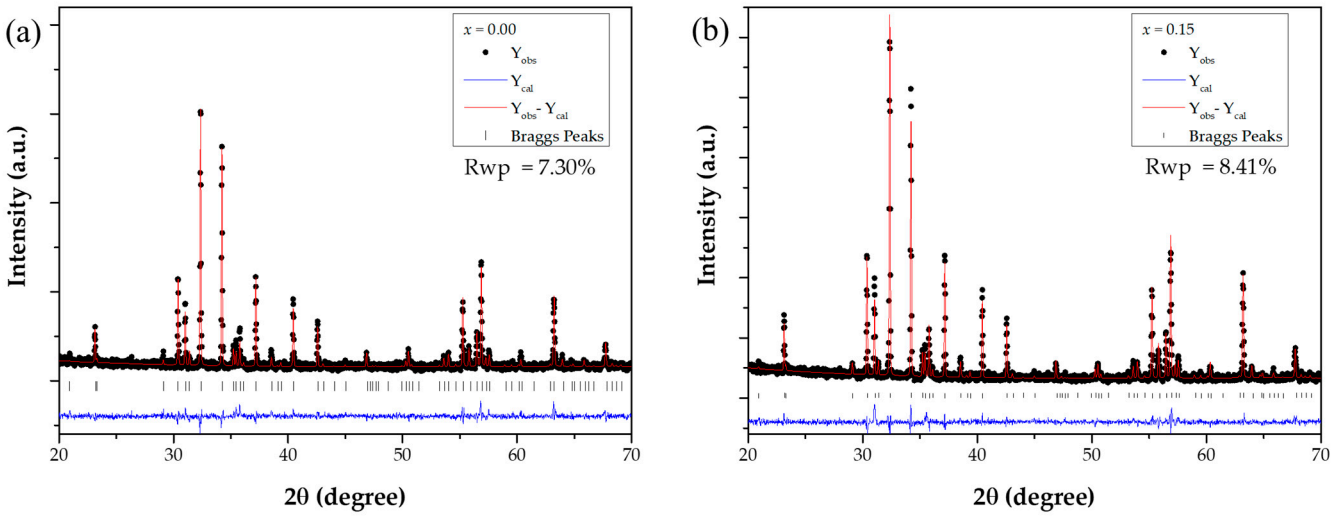


Figure 2. Rietveld analysis data of the $Sr_{1-x}La_xFe_{12-x}Co_xO_{19}$ samples sintered at 1300 °C for 2 h in air: (**a**) for x = 0.0, and (**b**) for x = 0.3.

Table 1. The lattice parameters a and c, c/a ratios, and cell volumes V_{cell} for the $Sr_{1-x}La_xFe_{12-x}Co_xO_{19}$ ($0.0 \leq x \leq 0.3$) samples sintered at 1300 °C for 2 h in air.

x	a (Å)	c (Å)	c/a	V_{cell} (Å^3)
0.0	5.8798 (2)	23.0624 (5)	3.922	690.470 (2)
0.1	5.8800 (3)	23.0510 (8)	3.919	690.405 (6)
0.15	5.8788 (2)	23.0450 (4)	3.918	689.871 (1)
0.2	5.8778 (3)	23.0321 (7)	3.918	689.162 (5)
0.25	5.8780 (4)	23.0202 (7)	3.916	688.803 (9)
0.3	5.8777 (2)	23.0313 (5)	3.918	689.032 (2)

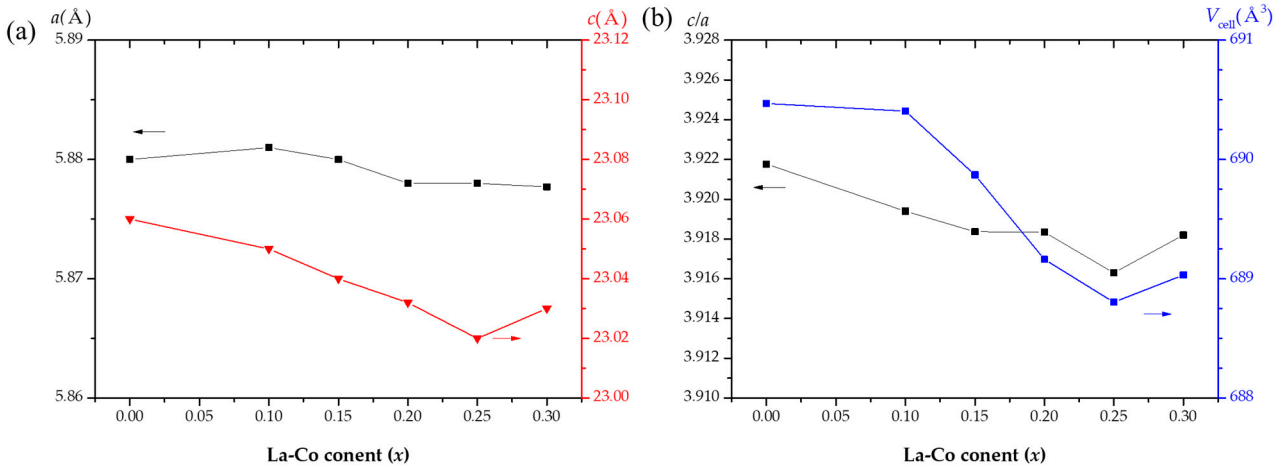
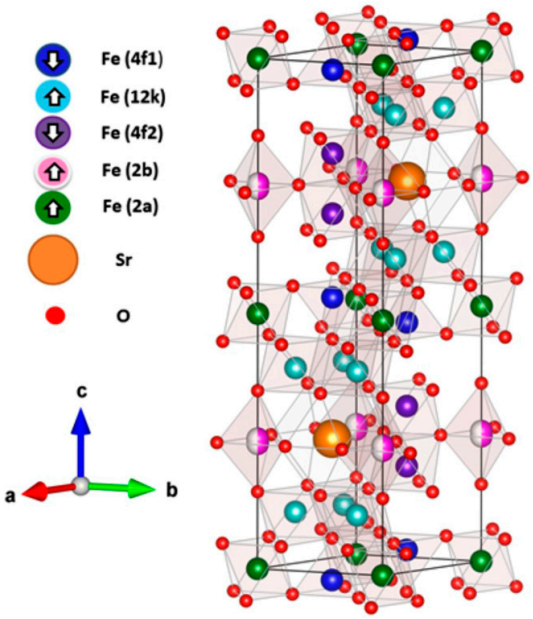


Figure 3. The lattice parameters (*a*, *c*) (**a**), unit cell volumes (V_{cell}) and the *c*/*a* ratios (**b**) for the $Sr_{1-x}La_xFe_{12-x}Co_xO_{19}$ ($0 \leq x \leq 0.3$) samples sintered at 1300 °C for 2 h in air.

Figure 3a shows the variation in the lattice parameters *a* and *c* with increasing *x*. Initially, *a* increases from *x* = 0.0 to 0.1 but then decreases up to *x* = 0.20; it then remains almost unaltered up to *x* = 0.3 while the lattice parameter *c* monotonously decreases with increasing *x* from 0.0 to 0.25, but it turns to an increase from *x* = 0.25 to 0.3. Since La^{3+} and Co^{2+} ions have been reported to replace the Sr^{2+} and Fe^{3+} sites, respectively [22,29], we sought to understand these behaviors by the smaller La^{3+} (1.22 Å) replacing the larger Sr^{2+} (1.31 Å) based on nine oxygen ion coordination and the larger Co^{2+} (0.75 Å) replacing the smaller Fe^{3+} (0.65 Å) based on six oxygen ion coordination [30]. As the same amount of La^{3+} was used to substitute for Sr^{2+} and Co^{2+} for Fe^{3+}, all samples were composed of the M-type single phase without any second phase, as shown in Figure 1b. Therefore, it is reasonable to assume that charge neutrality is always maintained. Considering only the influence of the size difference between the substituents (La^{3+} and Co^{2+}) and the original cation sites (Sr^{2+} and Fe^{3+}), the lattice constants *a* and *c* are expected to change consistently as a function of *x*. This consistency of the variations in *a* and *c* with *x* is observed for a wide range of *x* values, including the monotonous decrease in *c* up to *x* = 0.25 and the gradual decrease in a from *x* = 0.1 to 0.2, followed by almost constant values up to 0.25. The changes are surely due to the decreasing size effect of La^{3+} substitution for Sr^{2+}, which exceeds the increasing size effect of Co^{2+} for Fe^{3+}. However, in a limited range of *x* values, the variations in *a* and *c* with *x*, including the increase in *c* from *x* = 0.25 to 0.3 and also for the increase in a from *x* = 0.0 to 0.1, are unexplainable only with the size difference between the substituents (La^{3+}, Co^{2+}) and the original cation sites (Sr^{2+}, Fe^{3+}).

To understand the above peculiar variations of *a* and *c* with *x*, it is necessary to consider, in addition to the size difference, the effect of the valence difference on the lattice parameters, since the valence of the substituents (La^{3+}, Co^{2+}) is different from that of the original cation sites (Sr^{2+}, Fe^{3+}). To describe the cation sites within the unit cell of SrM hexaferrite, their locations must be specified as shown in Figure 4. The M-type hexaferrites exhibit a hexagonal structure composed of alternating layers of spinel (S, Fe_6O_8) and hexagonal (R, MFe_6O^{11}) blocks arranged as SRS*R*, where the asterisk (*) indicates a 180° rotation around the *c*-axis. The crystallographic sublattices of Fe^{3+} within the M-type structure are further divided into five distinct sites: 2*a*, 2*b*, $4f_1$, $4f_2$, and 12*k* sites. The magnetic moments of Fe^{3+} ions at the 12*k*, 2*a*, and 2*b* sites are oriented parallel to the *c*-axis (up-spin), while those at the $4f_1$ and $4f_2$ sites are oriented antiparallel (down-spin) [31].



Block	Sub-Lattice	Coordination	Cations	Spin
S	$4f_1$	Tetrahedral	2	↓
	2*a*	Octahedral	1	↑
R	$4f_2$	Octahedral	2	↓
	2*b*	Bi-pyramidal	1	↑
S-R	12*k*	Octahedral	6	↑

Figure 4. Crystallographic structure of $(SrFe_{12}O_{19})_2$. This figure was made using the TESTA program [32].

Using the above notations for Fe^{3+} sites, we can describe the peculiar variations in *a* and *c* with *x*. Initially, there is an increase in a from $x = 0.0$ to $x = 0.1$, as shown in Figure 3a. This is believed to be due to the increasing effect of larger Fe^{2+} ions (0.78 Å) transformed from smaller Fe^{3+} ions (0.65 Å) at the 2*a* site. The substitution of smaller La^{3+} (1.22 Å) by larger Sr^{2+} (1.31 Å) is seen to overcome this. Fe^{3+} ions at the 2*a* sites in La-substituted SrM samples have been converted to Fe^{2+} ions according to the Mössbauer analysis results of D. Seifert et al. [15]. Similarly, other research groups [23,33–35] have reported the presence of Fe^{2+} ions at the 2*a* sites, even in La-Co co-substituted SrM samples, while Co^{2+} is reported to substitute Fe^{3+} at the $4f_2$ and 2*a* sites. The presence of Fe^{2+} at the 2*a* sites in La-Co co-substituted SrM is often attributed to a non-uniform distribution of La^{3+} and Co^{2+} substituents within the crystal structure. This results in a transformation from Fe^{3+} to Fe^{2+} for local charge neutrality. However, the lattice parameters of *a* and *c* in Co-substituted SrM samples are reported to be almost unchanged [36] or slightly increased [37] with an increase in the amount of Co substituent. To maintain charge neutrality without producing Fe^{2+}, it is necessary to generate vacancies in the oxygen ion. Therefore, the effect of Co substitution on the lattice parameters *a* and *c* is considered insignificant. This is because the increase caused by Co^{2+} substitution for Fe^{3+} can be counteracted by the generation of oxygen ion vacancies. The initial increase in a and the monotonous decrease in *c* from $x = 0.0$ to $x = 0.1$ are well consistent with the previous report by T. Waki et al. [17], although their values are somewhat different. However, in the *x* region of 0.1–0.3, unlike our samples, their lattice constant a values continuously increase with increasing *x* due to a gradual decrease in the Co/La molar ratio below 1.0. Figure 3a indicates that the presence of Fe^{2+} at the 2*a* site has a significant effect on the lattice parameter *a*, while its effect on the lattice parameter *c* is negligible up to $x = 0.25$. Additionally, the upturn in the lattice parameter *c* at $x = 0.3$, deviating from its monotonous decrease up to $x = 0.25$, is attributable to a change in the occupancy of Co^{2+} substituent at the 2*a* site, affecting the formation of Fe^{2+} and causing a shift in the oxygen vacancy positions. This peculiar behavior is also observed for the La-Co

substituted SrM sample with x = 0.4, prepared using additives reported by K. Ida et al. [22], although they never discussed the reason for its occurrence.

In contrast to the variations in lattice parameters a and c with x shown in Figure 3a, T.T. Loan et al. [23] reported different behaviors for La-Co co-substituted SrM powder synthesized by the sol–gel method and subsequently fired at 900 °C for 2 h in air. Their values for a and c slightly decreased from x = 0.0 to 0.1 and then gradually increased up to 0.2. Additionally, their values were much lower than ours, except for the composition of x = 0.2, which showed almost the same values. This discrepancy may be attributed to the significant difference in firing temperatures. However, additional experiments are necessary to confirm this.

Figure 5 shows SEM micrographs and average grain sizes of $Sr_{1-x}La_xFe_{12-x}Co_xO_{19}$ samples ($0.0 \leq x \leq 0.3$). The grains have hexagonal plate shapes, and both the average plate width and thickness were measured on the micrographs. The average width and thickness values are approximately 2–4 μm and 0.7–1.5 μm, respectively. It is worth noting that the single domain size (d_{sd}) of SrM hexaferrite is approximately 940 nm [1]. Since most of the grains shown in Figure 5 are larger than d_{sd}, they are likely composed of multi-domain structures. It appears that there is no significant difference in microstructure between the samples. From Figure 5g, it was observed that the morphological aspect ratios, defined as the average plate width over average plate thickness, sharply decrease from 3.80 to 2.45 as x increases from 0.0 to 0.10. The aspect ratio then increases to 3.66 for x = 0.15, and gradually decreases to 2.08 for x = 0.30. The aspect ratios versus x are not presented here.

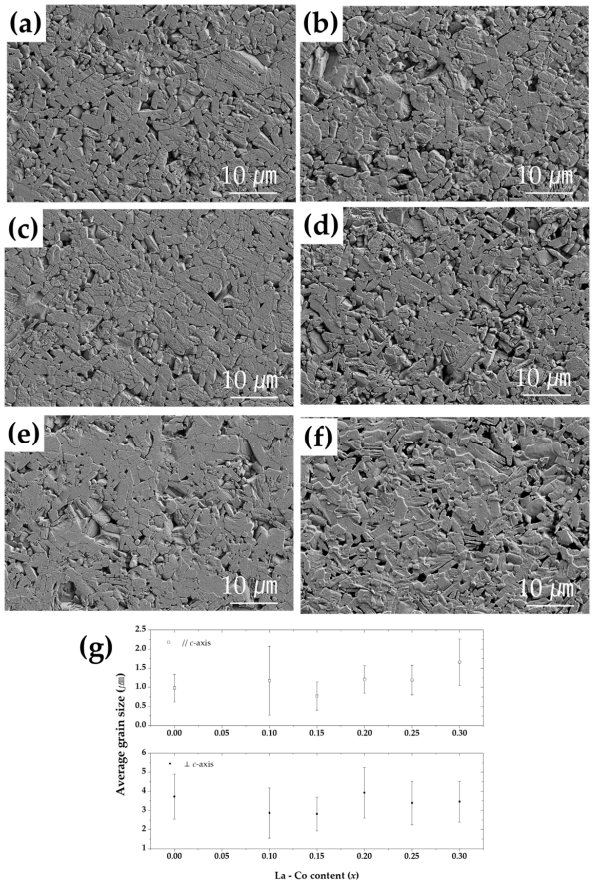


Figure 5. SEM micrographs of the $Sr_{1-x}La_xFe_{12-x}Co_xO_{19}$ samples with (**a**) x = 0.0, (**b**) x = 0.1, (**c**) x = 0.15, (**d**) x = 0.2, (**e**) x = 0.25, (**f**) x = 0.3, and (**g**) average grain size (parallel and perpendicular to c-axis) of the samples.

3.2. Magnetic Property Analysis

The initial magnetization curves of all samples are shown in Figure 6. From these initial magnetization curves, the M_S and H_a values of samples could be calculated using the law of approach to saturation (LAS) [38] given by the following equation,

$$M = M_s\left(1 - \frac{A}{H} - \frac{B}{H^2}\right) + \chi_p H \quad (2)$$

where M is magnetization induced by an applied magnetic field H, the parameter A is related to the inhomogeneity of a material, B is the anisotropy parameter related to the magnetocrystalline anisotropy, and χ_p is the high field susceptibility [39]. The inhomogeneity parameter A is a factor that relies on the influence of vacancies, lattice distortion, and local concentration fluctuation that hinders the domain wall motions. The calculation of A/H term is valid in a relatively low magnetic field range, where magnetic domain wall motion contributes to M. The domain wall motion, however, is non-negligible even in a relatively high field. R. Groessinger [38] reported that A had about 250 Oe in the case of BaM hexaferrite.

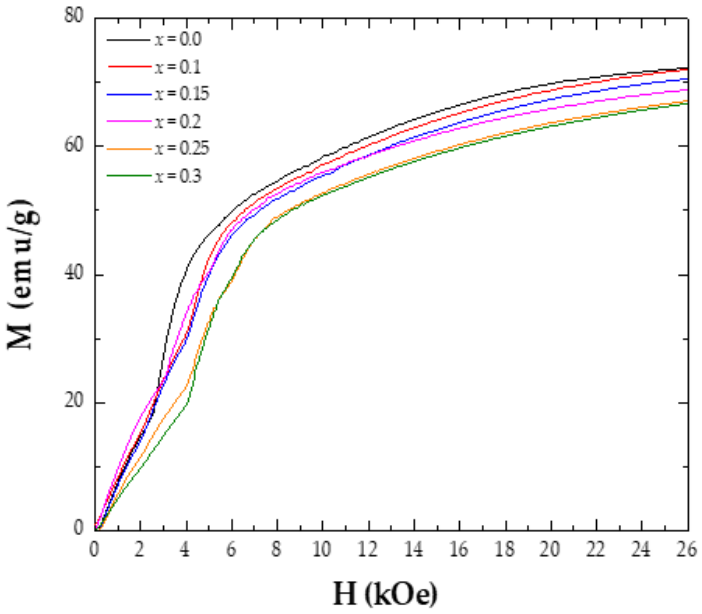


Figure 6. The initial magnetization curves for the $Sr_{1-x}La_xFe_{12-x}Co_xO_{19}$ polycrystalline samples with x = 0, 0.1, 0.15, 0.2, 0.25, and 0.3.

For a hexagonal crystal structure exhibiting uniaxial anisotropy, the B parameter can be expressed as follows:

$$B = \frac{H_a^2}{15} \quad (3)$$

Since the χ_p is negligibly small compared to B in the H-field region of the consideration, Equation (2) can be approximated by the following equation:

$$M = M_s\left\{1 - \frac{A}{H} - \frac{1}{15}\left(\frac{H_a}{H}\right)^2\right\} \quad (4)$$

Then, the M_S value can be obtained from the linear part on M vs. $1/H$ curves. The A and H_a values can be calculated by fitting Equation (4) to the measured $M(H)$ curves.

The procedure for fitting Equation (4) to the measured $M(H)$ data is as follows. For example, Figure 7a presents the fitting results for the sample with x = 0.15, which is representative of all samples. The black (A), blue (R^2), and red (H_a) lines represent the fitted

curves calculated in the field region of 12–26 kOe, respectively. R^2 is the output statistical parameter that represents the goodness of the curve fitting, and it is highly reliable when R^2 is higher than 0.990. Figure 7 shows the results of fixing the maximum field value and widening it to the lower field region. The values of A, H_a, and R^2 are calculated and plotted. A gradually increases and becomes positive below 15 kOe, while both H_a and R^2 gradually decrease. In the field region where A is about 200–300, R^2 shows a value of 0.990 or higher, and H_a shows a value of 21.7 kOe. Without A, the LAS fitting to the experimental $M(H)$ values in the same field region resulted in a relatively high H_a of 23.1 kOe and a low R^2 value of 0.9858, indicating a worse LAS fitting. Therefore, the field region of 12–26 kOe was selected for fitting with Equation (4). As shown in Figure 7b, the red LAS fitting curve fits well with the measured data in the selected field region. However, the red curve fitted to the data deviates significantly from the measured values at the lower field region of $H \leq 12$ kOe. Table 2 lists the calculated values for M_S, H_a, A, and R^2.

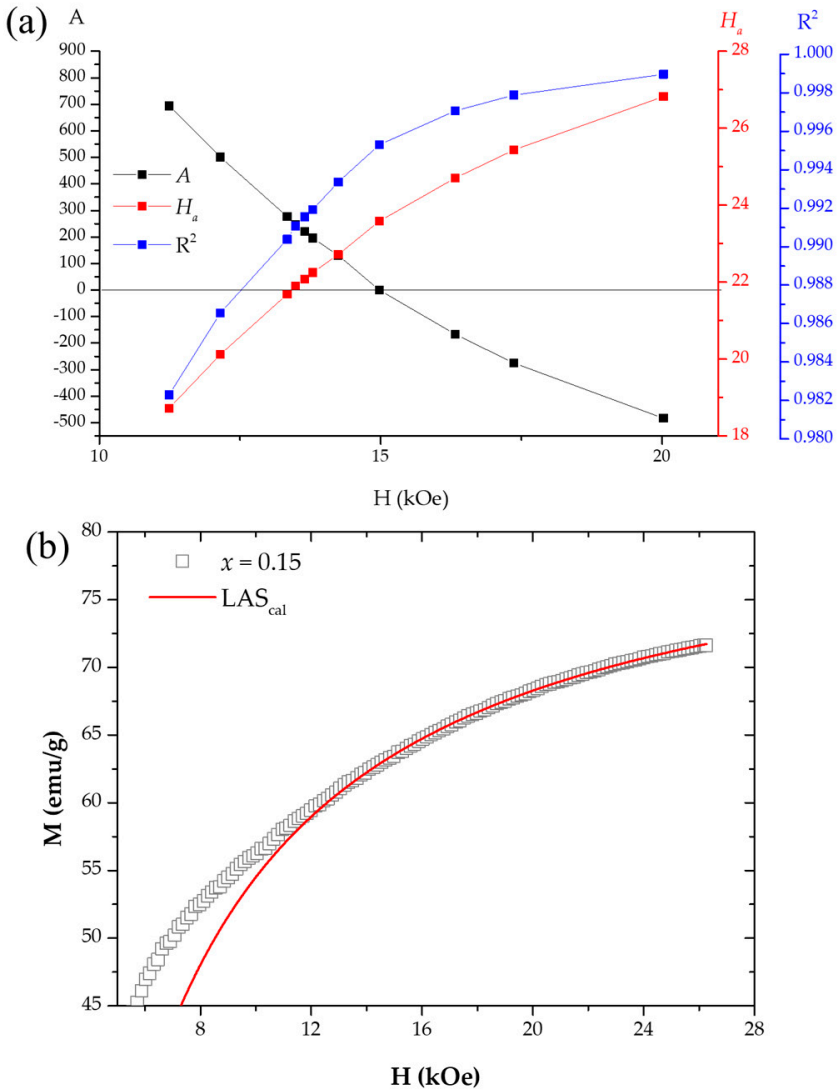


Figure 7. Fitting of the law of approach to saturation (LAS) to experimental data for $Sr_{1-x}La_xFe_{12-x}Co_xO_{19}$ (x = 0.15) samples: linear fitting by Equation (2) for (**a**) M_s, A, H_a, and R^2, and (**b**) non-linear fitting by Equation (1).

Table 2. The $M_{@26kOe}$, H_{ci}, M_s, H_a, A, field region for fitting, and R^2 values for the $Sr_{1-x}La_xFe_{12-x}Co_xO_{19}$ ($0.0 \leq x \leq 0.3$) samples sintered at 1300 °C for 2 h in air. The calculated values are presented with error range.

x	$M_{@26kOe}$ (emu/g)	H_{ci} (kOe)	M_s (emu/g)	H_a (kOe)	A (Oe)	Field Region for Fitting (kOe)	R^2
0.0	72.27	2.68 ± 0.14	75.90 ± 0.04	20.1 ± 1.3	242	12–26	0.99265
0.1	72.04	2.99 ± 0.09	75.46 ± 0.04	21.5 ± 1.2	245	14–26	0.99267
0.15	70.68	3.32 ± 0.09	73.58 ± 0.03	21.5 ± 1.1	255	14–26	0.99275
0.2	68.92	3.45 ± 0.18	73.42 ± 0.04	21.6 ± 1.0	245	15–26	0.99277
0.25	67.18	3.71 ± 0.10	72.50 ± 0.05	23.9 ± 1.1	252	16–26	0.99332
0.3	66.80	3.99 ± 0.10	72.07 ± 0.05	24.7 ± 1.1	255	17–26	0.99329

The magnetic hysteresis loops of samples are shown in Figure 8. From these loops, the maximum M values measured at H = 26 kOe ($M_{@26kOe}$) and intrinsic coercivity (H_{ci}) were obtainable. These values are also listed in Table 2. The M_S, $M_{@26kOe}$, H_a, and H_{ci} values for all samples in this table are plotted as a function of x as shown in Figure 9.

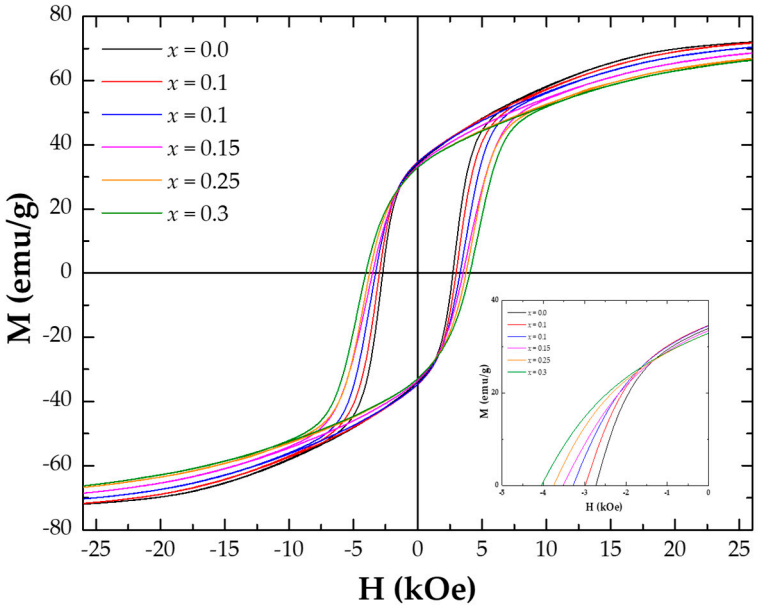


Figure 8. The *M*-*H* curves for the $Sr_{1-x}La_xFe_{12-x}Co_xO_{19}$ samples with x = 0, 0.1, 0.15, 0.2, 0.25, and 0.3 sintered at 1300 °C for 2 h in air. The second quadrants of *M*-*H* curves are placed as an inset.

The effect of La-Co substitution (x) on the magnetic properties of as-sintered samples can be understood as follows. As shown in Table 2 and Figure 9a, the values of M_S and $M_{@2.6kOe}$ gradually decrease from 75.90 to 72.07 emu/g and from 72.27 to 66.80 emu/g, respectively, as x increases from 0.0 to 0.3. This suggests that Co^{2+} replaces Fe^{3+} at the $4f_2$ site, while Co^{2+}/Fe^{2+} substitution occurs at the 2*a* site, leading to the gradual decrease in M_S. The M_S dependency of x for our samples agrees well with that reported for powder samples prepared by the sol–gel process and subsequent firing at 900 °C for 24 h in air [20]. Specifically, M_S decreases as x increases. However, the M_S vs. x behavior reported by T. T. Loan et al. [23] differs from ours, despite their use of the sol–gel process and subsequent firing at 900 °C for 2 h in air to prepare powder samples with x = 0.0 and 0.05. Lower M_S values for samples with x = 0.0 and 0.05 may be due to the presence of small nanoparticles (<50 nm) exhibiting superparamagnetism, as observed in their SEM micrographs. In contrast, the larger particles in samples with $x \geq 0.1$ exhibit a decreasing behavior in M_S with increasing x, similar to our sintered bulk samples.

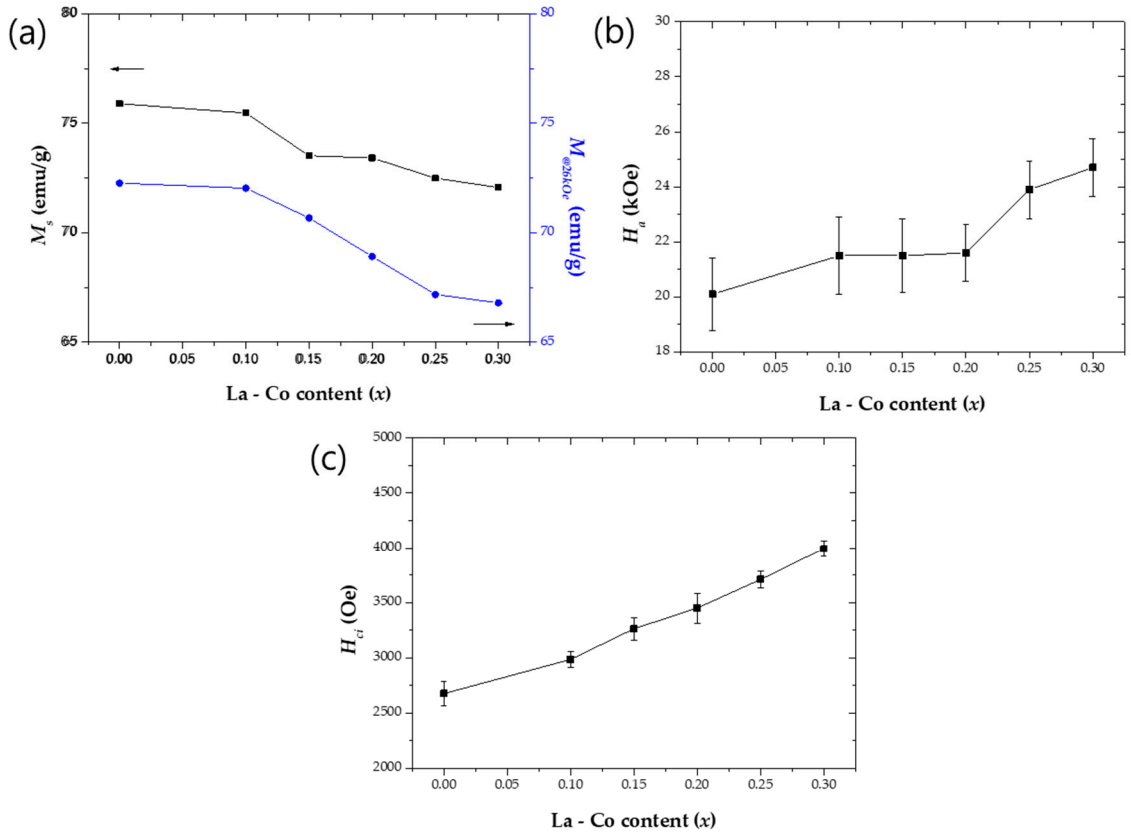


Figure 9. The plots of (**a**) M_s, and $M_{@26kOe}$ vs. x, (**b**) H_a vs. x, and (**c**) H_{ci} vs. x, for $Sr_{1-x}La_xFe_{12-x}Co_xO_{19}$ ($0 \leq x \leq 0.3$) samples sintered at 1300 °C for 2 h in air.

Table 2 and Figure 9b show that the value of H_a increases from 20.1 to 21.5 kOe as x increases from 0.00 to 0.10. It then slightly increases to 21.6 kOe up to x = 0.20, followed by a further increase to 24.7 kOe up to x = 0.30. These variations in x are almost inversely proportional to the variation in the c/a values with x shown in Figure 3b, except for the H_a value at x = 0.3. Peng et al. [19] reported that H_a can be increased due to a gradual decrease in crystallographic symmetry with increasing x in La-Co co-substituted SrM. However, H_a increases even as c/a increases at x = 0.3. This may be due to the increased occupancy of Co^{2+} at the 2*a* site, as discussed above in relation to the increase in c. The behavior of H_a increasing with x is similar to that reported by T. Kikuchi et al. [20]. However, our H_a values are approximately 16% higher than theirs. They evaluated their H_a values not from initial magnetization curves, but from magnetic hysteresis curves measured only up to the applied field of 16 kOe. Furthermore, they did not take the A factor in Equation (4) into account for their calculation of M_S and H_a values, which might be responsible for their lower M_S and H_a values compared to our data.

The H_{ci} values of our polycrystalline samples were experimentally obtained from the *M*-*H* hysteresis curves. At least three samples of each composition were measured. The average H_{ci} values and their standard deviations are shown in Figure 9c. The average H_{ci} values increase from 2.68 to 3.99 kOe as x increases. The H_{ci} values show significant variation with a large standard deviation for the samples with x = 0.10 and 0.15, resulting in relatively large error bars. However, the standard deviation decreases as x increases further. As x increases, the homogeneity of La-Co substituents within the crystal structure may increase, resulting in a decrease in the standard deviation of H_{ci}. The variation in H_{ci} with x in Figure 9c can be explained by H_a and microstructure, which includes the grain size, shape, and density of sintered samples. The increase in H_{ci} with increasing x is mainly due to the increase in H_a. There is no significant variation in the microstructures of samples with x, as shown in Figure 4.

4. Conclusions

Without the use of sintering additives, La-Co co-substituted SrM single phases having the compositions of $Sr_{1-x}La_xFe_{12-x}Co_xO_{19}$ ($0.0 \leq x \leq 0.3$) are obtainable from polycrystalline bulk samples prepared by solid-state reaction in air by employing proper processing conditions. Therefore, we could accurately identify the effects of La-Co co-substitution on their structural and intrinsic magnetic properties up to the composition of $x = 0.3$. The decrease in c/a ratios and V_{cell} values with increasing x are surely due to the decreasing size effect of La^{3+} substitution at the Sr^{2+} site, exceeding the increasing size effect of Co^{2+} and Fe^{2+} occupation at the Fe^{3+} site up to $x = 0.25$. However, the upturn in the lattice constant c from $x = 0.25$ to 0.3 is probably due to a rapid increase in Co^{2+} occupancy of the 2*a* site compared to that of the $4f_2$ site, which requires further study. With increasing x from 0.0 to 0.3, M_S decreases from 75.90 to 72.07 emu/g because decreasing effect by Co^{2+} and Fe^{2+} occupation at the 2*a* site (up-spin) becomes larger than increasing effect by Co^{2+} occupation at the $4f_2$ site (down-spin); H_a increases from 20.1 to 24.7 kOe, probably due to a lowering of the lattice symmetry, and causes a continuous increase in H_{ci} from 2.68 to 3.99 kOe. The significant difference in the structural and intrinsic magnetic properties between our bulk samples sintered at 1300 °C and sol–gel processed powder samples fired at 900 °C without additives may be due to a large difference in the firing temperatures, of which identification also requires further study.

Author Contributions: Conceptualization, K.L.; funding acquisition, S.-I.Y.; investigation, K.L. and S.-I.Y.; methodology K.L.; project administration, S.-I.Y.; software, K.L.; supervision, Y.-M.K. and S.-I.Y.; writing—original draft, K.L. All authors have read and agreed to the published version of the manuscript.

Funding: This research was supported by National R&D Program through the National Research Foundation of Korea (NRF) and was funded by the Ministry of Science and ICT (2020M3H4A2084420).

Institutional Review Board Statement: Not applicable.

Informed Consent Statement: Not applicable.

Data Availability Statement: The data presented in this study are available on request from the corresponding author. The data are not publicly available due to privacy.

Acknowledgments: The authors are also grateful to Union Materials Corp. in Pohang, Republic of Korea for the supporting of raw materials for magnet fabrication.

Conflicts of Interest: The authors declare no conflicts of interest.

References

1. Pullar, R.C. Hexagonal ferrites: A review of the synthesis, properties and applications of hexaferrite ceramics. *Prog. Mater. Sci.* **2012**, *57*, 1191–1334. [CrossRef]
2. Brawn, R. The crystal structure of a new group of ferromagnetic compounds. *Philips Res. Rep.* **1957**, *12*, 491–548.
3. Gorter, E. Chemistry and magnetic properties of some ferrimagnetic oxides like those occurring in nature. *Adv. Phys.* **1957**, *6*, 336–361. [CrossRef]
4. Cochardt, A. Effects of sulfates on the properties of strontium ferrite magnets. *J. Appl. Phys.* **1967**, *38*, 1904–1908. [CrossRef]
5. Shirk, B.; Buessem, W. Temperature dependence of M_s and K_1 of $BaFe_{12}O_{19}$ and $SrFe_{12}O_{19}$ single crystals. *J. Appl. Phys.* **1969**, *40*, 1294–1296. [CrossRef]
6. Ormerod, J. Permanent magnet materials. In Proceedings of the IEE Colloquium on New Permanent Magnet Materials and Their Applications, London, UK, 9 January 1989.
7. Cullity, B.D.; Graham, C.D. *Introduction to Magnetic Materials*; John Wiley & Sons: Hoboken, NJ, USA, 2011.
8. Kools, F.; Morel, A.; Grossinger, R.; Le Breton, J.M.; Tenaud, P. LaCo-substituted ferrite magnets, a new class of high-grade ceramic magnets; intrinsic and microstructural aspects. *J. Magn. Magn. Mater.* **2002**, *242*, 1270–1276. [CrossRef]
9. Sahu, P.; Tripathy, S.N.; Pattanayak, R.; Muduli, R.; Mohapatra, N.; Panigrahi, S. Effect of grain size on electric transport and magnetic behavior of strontium hexaferrite ($SrFe_{12}O_{19}$). *Appl. Phys. A* **2017**, *123*, 3. [CrossRef]
10. O'Handley, R.C. *Modern Magnetic Materials: Principles and Applications*; John Wiley & Sons: Hoboken, NJ, USA, 1999.
11. Chavan, V.C.; Shirsath, S.E.; Mane, M.L.; Kadam, R.; More, S.S. Transformation of hexagonal to mixed spinel crystal structure and magnetic properties of Co^{2+} substituted $BaFe_{12}O_{19}$. *J. Magn. Magn. Mater.* **2016**, *398*, 32–37. [CrossRef]

12. Vinnik, D.; Zhivulin, V.; Starikov, A.Y.; Gudkova, S.; Trofimov, E.; Trukhanov, A.; Trukhanov, S.; Turchenko, V.; Matveev, V.; Lahderanta, E. Influence of titanium substitution on structure, magnetic and electric properties of barium hexaferrites $BaFe_{12-x}Ti_xO_{19}$. *J. Magn. Magn. Mater.* **2020**, *498*, 166117. [CrossRef]
13. Dai, Y.; Lan, Z.; Wu, C.; Yang, C.; Yu, Z.; Guo, R.; Wang, W.; Chen, C.; Liu, X.; Jiang, X. Tailoring magnetic properties of Al-substituted M-type strontium hexaferrites. *Appl. Phys. A* **2018**, *124*, 842. [CrossRef]
14. Baykal, A.; Sözeri, H.; Güngüneş, H.; Auwal, I.; Shirsath, S.E.; Sertkol, M.; Amir, M. Synthesis and Structural and Magnetic Characterization of $BaZn_xFe_{12-x}O_{19}$ Hexaferrite: Hyperfine Interactions. *J. Supercond. Nov. Magn.* **2017**, *30*, 1585–1592. [CrossRef]
15. Seifert, D.; Töpfer, J.; Langenhorst, F.; Le Breton, J.-M.; Chiron, H.; Lechevallier, L. Synthesis and magnetic properties of La-substituted M-type Sr hexaferrites. *J. Magn. Magn. Mater.* **2009**, *321*, 4045–4051. [CrossRef]
16. Grossinger, R.; Kupferling, M.; Blanco, J.T.; Wiesinger, G.; Muller, M.; Hilscher, G.; Pieper, M.; Wang, J.; Harris, I. Rare earth substitutions in M-type ferrites. *IEEE Trans. Magn.* **2003**, *39*, 2911–2913. [CrossRef]
17. Waki, T.; Okazaki, S.; Tabata, Y.; Kato, M.; Hirota, K.; Nakamura, H. Effect of oxygen potential on Co solubility limit in La–Co co-substituted magnetoplumbite-type strontium ferrite. *Mater. Res. Bull.* **2018**, *104*, 87–91. [CrossRef]
18. Yuping, L.; Yunfei, W.; Daxin, B. Enhanced coercivity of La–Co substituted Sr–Ca hexaferrite fabricated by improved ceramics process. *J. Mater. Sci. Mater. Electron.* **2016**, *27*, 4433–4436. [CrossRef]
19. Peng, L.; Li, L.; Wang, R.; Hu, Y.; Tu, X.; Zhong, X. Effect of La–CO substitution on the crystal structure and magnetic properties of low temperature sintered $Sr_{1-x}La_xFe_{12-x}Co_xO_{19}$ (x = 0–0.5) ferrites. *J. Magn. Magn. Mater.* **2015**, *393*, 399–403. [CrossRef]
20. Kikuchi, T.; Nakamura, T.; Yamasaki, T.; Nakanishi, M.; Fujii, T.; Takada, J.; Ikeda, Y. Magnetic properties of La–Co substituted M-type strontium hexaferrites prepared by polymerizable complex method. *J. Magn. Magn. Mater.* **2010**, *322*, 2381–2385. [CrossRef]
21. Liu, X.; Hernández-Gómez, P.; Huang, K.; Zhou, S.; Wang, Y.; Cai, X.; Sun, H.; Ma, B. Research on La^{3+}–Co^{2+}-substituted strontium ferrite magnets for high intrinsic coercive force. *J. Magn. Magn. Mater.* **2006**, *305*, 524–528. [CrossRef]
22. Iida, K.; Minachi, Y.; Masuzawa, K.; Kawakami, M.; Nishio, H.; Taguchi, H. High-performance ferrite magnets: M-type Sr-ferrite containing lanthanum and cobalt. *J. Magn. Soc. Jpn.* **1999**, *23*, 1093–1096. [CrossRef]
23. Loan, T.T.; Nga, T.T.V.; Duong, N.P.; Soontaranon, S.; Hien, T.D. Influence of Structure and Oxidation State on Magnetic Properties of $Sr_{1-x}La_xFe_{12-x}Co_xO_{19}$ Nanoparticles Prepared by Sol–Gel Combustion Method. *J. Electron. Mater.* **2017**, *46*, 3396–3405. [CrossRef]
24. Moon, K.-S.; Yu, P.-y.; Kang, Y.-M. Microstructure and magnetic properties of La-Ca-Co substituted M-type Sr-hexaferrites with controlled Si diffusion. *Appl. Sci.* **2020**, *10*, 7570. [CrossRef]
25. Li, X.; Yang, W.; Bao, D.; Meng, X.; Lou, B. Influence of Ca substitution on the microstructure and magnetic properties of SrLaCo ferrite. *J. Magn. Magn. Mater.* **2013**, *329*, 1–5. [CrossRef]
26. Solovyova, E.; Pashkova, E.; Ivanitski, V.; Belous, A. Mössbauer and X-ray diffraction study of Co^{2+}–Si^{4+} substituted M-type barium hexaferrite $BaFe_{12-2x}Co_xSi_xO_{19\pm\gamma}$. *J. Magn. Magn. Mater.* **2013**, *330*, 72–75. [CrossRef]
27. Yao, Y.; Hrekau, I.; Tishkevich, D.; Zubar, T.; Turchenko, V.; Lu, S.; Silibin, M.; Migas, D.; Sayyed, M.; Trukhanov, S. Correlation of the chemical composition, phase content, structural characteristics and magnetic properties of the Bi-substituted M-type hexaferrites. *Ceram. Int.* **2023**, *49*, 37009–37016. [CrossRef]
28. Shimoda, A.; Takao, K.; Uji, K.; Waki, T.; Tabata, Y.; Nakamura, H. Flux growth of magnetoplumbite-type strontium ferrite single crystals with La–Co co-substitution. *J. Solid State Chem.* **2016**, *239*, 153–158. [CrossRef]
29. Mangai, K.A.; Selvi, K.T.; Priya, M.; Sureshkumar, P.; Rathnakumari, M. Impedance and modulus spectroscopy studies of cobalt substituted strontium hexaferrite ceramics. *J. Mater. Sci. Mater. Electron.* **2017**, *28*, 13445–13454. [CrossRef]
30. Shannon, R.D. Revised effective ionic radii and systematic studies of interatomic distances in halides and chalcogenides. *Acta Crystallogr. Sect. A Cryst. Phys. Diffr. Theor. Gen. Crystallogr.* **1976**, *32*, 751–767. [CrossRef]
31. Smit, J.; Wijn, H. *Ferrites*; Philips Technical Library: Eindhoven, The Netherlands, 1959; Volume 278.
32. Momma, K.; Izumi, F. VESTA 3 for three-dimensional visualization of crystal, volumetric and morphology data. *J. Appl. Crystallogr.* **2011**, *44*, 1272–1276. [CrossRef]
33. Wiesinger, G.; Müller, M.; Grössinger, R.; Pieper, M.; Morel, A.; Kools, F.; Tenaud, P.; Le Breton, J.; Kreisel, J. Substituted ferrites studied by nuclear methods. *Phys. Status Solidi (a)* **2002**, *189*, 499–508. [CrossRef]
34. Morel, A.; Le Breton, J.; Kreisel, J.; Wiesinger, G.; Kools, F.; Tenaud, P. Sublattice occupation in $Sr_{1-x}La_xFe_{12-x}Co_xO_{19}$ hexagonal ferrite analyzed by Mössbauer spectrometry and Raman spectroscopy. *J. Magn. Magn. Mater.* **2002**, *242*, 1405–1407. [CrossRef]
35. Lechevallier, L.; Le Breton, J.; Teillet, J.; Morel, A.; Kools, F.; Tenaud, P. Mössbauer investigation of $Sr_{1-x}La_xFe_{12-y}Co_yO^{19}$ ferrites. *Physica B Condens. Matter* **2003**, *327*, 135–139. [CrossRef]
36. Tran, N.; Choi, Y.; Phan, T.; Yang, D.; Lee, B. Electronic structure and magnetic and electromagnetic wave absorption properties of $BaFe_{12-x}Co_xO_{19}$ M-type hexaferrites. *Curr. Appl. Phys.* **2019**, *19*, 1343–1348. [CrossRef]
37. Altaf, F.; Atiq, S.; Riaz, S.; Naseem, S. Synthesis of Co-doped Sr-hexaferrites by Sol-gel Auto-combustion and its Electrical Characterization. *Mater. Today Proc.* **2015**, *2*, 5548–5551. [CrossRef]

38. Grossinger, R. A Critical-Examination of the Law of Approach to Saturation. 1. Fit Procedure. *Phys. Status Solidi A* **1981**, *66*, 665–674. [CrossRef]
39. Grössinger, R. Correlation between the inhomogeneity and the magnetic anisotropy in polycrystalline ferromagnetic materials. *J. Magn. Magn. Mater.* **1982**, *28*, 137–142. [CrossRef]

Disclaimer/Publisher's Note: The statements, opinions and data contained in all publications are solely those of the individual author(s) and contributor(s) and not of MDPI and/or the editor(s). MDPI and/or the editor(s) disclaim responsibility for any injury to people or property resulting from any ideas, methods, instructions or products referred to in the content.